Christin Bald, Robert Bergholz, and Gerhard Schmidt*

Automatic Localization of an Ultrasound Probe with the Help of Magnetic Sensors

https://doi.org/10.1515/cdbme-2022-1081

Abstract: Ultrasound measurements are a widely used instrument in clinical practice. For later traceability of the images, the position (and orientation) of the ultrasound probe must be recorded during the measurement. Until now this has to be done manually by the physician. An easier and more accurate approach would be the automatic tracking of the ultrasound probe. This contribution shows a first approach for automatically localizing the ultrasonic head during measurement. The proposed method is based on coils surrounding the patient bed and a 3D magnetic sensor placed on the ultrasound head. Besides some pre- and postprocessing steps, the proposed localization algorithm is based on trilateration followed by a least mean squares approach for refinement of the estimation. In a first proof-of-concept measurement with fixed positions and orientations of the ultrasound head a mean accuracy of $2.85\,\mathrm{cm}$ and 8.94° was achieved. Additionally, a measurement with a moving ultrasound head is presented to demonstrate the real-time capability of the system. Finally, future steps for improving the automatic measurement are discussed, including a graphical user interface for the physician and the use of magnetoelectric sensors for measurement.

Keywords: Magnetic localization; Ultrasound head localization; Real-time localization; Inverse solution; Magnetic sensors

1 Introduction

Ultrasound measurements are a frequently used tool in everyday clinical practice. Up to now, the position and orientation of the ultrasound head have to be noted by hand by the clinician. Due to the busy clinical routine, the markings are sometimes incorrect or not precise enough. Thus, an automatic labeling process of the position and orientation of the ultrasound probe would be highly beneficial. Tracking of an ultrasound probe has been done in various ways, e.g. using optical [1] or electromagnetic [2, 3] tracking devices. Due to the clear advantage that no line-of-sight is necessary using (electro-) magnetic tracking, this method is widely used [3]. This contribution aims to provide a complete and robust localization chain for magnetic tracking of an ultrasound probe working in real-time, which can be applied to every kind of magnetic (3D) sensor. In addition, it serves as a preliminary work for an extension towards magnetoelectric sensors [4], which are cost-efficient in production, highly sensitive, and very small and could thus easily be integrated in an ultrasound head.

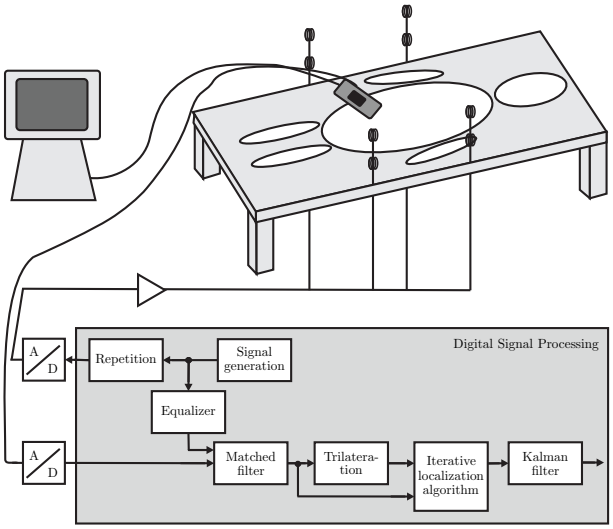

Fig. 1: Proposed method for localizing the ultrasound probe. The patient bed is equipped with coils, while a 3D magnetic sensor is placed on the ultrasound head. The signals measured by the magnetic sensor are digitally processed. Due to the localization of the magnetic 3D sensor, the position and orientation of the ultrasound head can be determined.

2 Proposed Method

As a first draft, a 3D magnetic sensor is fixed on the ultrasound head with coils placed around the patient bed transmitting orthogonal signals as shown in Fig. 1. With localizing the magnetic 3D sensor, the position and orientation of the ultrasound head can be determined. For the magnetic 3D sensor, 1D fluxgate sensors (type FLC 100 and FLC 100-T by

***Corresponding author: Gerhard Schmidt,** Digital Signal Processing and System Theory, Institute of Electrical Engineering and Information Technology, Faculty of Engineering, Christian-Albrechts-Universität zu Kiel, Kaiserstraße 2, Kiel, Germany, e-mail: gus@tf.uni-kiel.de
Christin Bald, Digital Signal Processing and System Theory, Institute of Electrical Engineering and Information Technology, Faculty of Engineering, Christian-Albrechts-Universität zu Kiel, Kiel, Germany
Robert Bergholz, Pediatric Surgery, Faculty of Medicine, Christian-Albrechts-Universität zu Kiel, Kiel, Germany

Stefan Mayer Instruments [5]) are combined such, that each sensor is pointing in another orthogonal direction. Although there are small offsets between the sensor positions, the magnitude of the magnetic field at the center of the array can be measured approximately. Due to the sensor's -3 dB bandwidth of 1 kHz [5], an FDMA (Frequency Devision Multiple Access) approach can be used, i.e. exciting all coils simultaneously. Hann windowed chirp signals of 30 Hz bandwidth and a length of 96 ms are created between 610 Hz and 990 Hz with a distance of 20 Hz between the individual signals. Due to the known arrangement of the sensors to each other, more known input variables are available to solve the inverse problem. With $N_\mathrm{c} = 8$ coils and $N_\mathrm{s} = 3$ used sensors this leads to a total amount of $N_\mathrm{in} = N_\mathrm{c} N_\mathrm{s} = 24$ input variables used in this study.

2.1 Localization Algorithm

The localization pipeline used in this contribution is shown in the lower part of Fig. 1. The whole localization procedure (except for trilateration) was presented and explained in detail in [6]. First, the sensor input signals are matched filtered for separating the coil signals from the mixed sensor input signals. The used impulse responses of the matched filters are the mirrored and equalized excitations signals [6]. To compensate for phase differences, ± 10 samples were considered around the delay offset. This serves as the input for the localization algorithm. In general, the inverse problem is solved using a least mean squares like approach as presented in [4, 6]. When localizing in the three-dimensional space (six unknown variables) with a sensor array the computational complexity increases drastically and the real-time capability of the system is endangered. Thus the localization approach is slightly modified by starting with a first guess of the position of the 3D sensor based on trilateration [7] (but with N_c variables):

$$\hat{\boldsymbol{p}}(k) = \boldsymbol{D}^\dagger \, \boldsymbol{u}(k) \tag{1}$$

with $\boldsymbol{D}^\dagger$ denoting the pseudoinverse of the matrix

$$\boldsymbol{D} = 2 \begin{bmatrix} p_{\mathrm{c}_x,2} - p_{\mathrm{c}_x,1} & p_{\mathrm{c}_y,2} - p_{\mathrm{c}_y,1} & p_{\mathrm{c}_z,2} - p_{\mathrm{c}_z,1} \\ p_{\mathrm{c}_x,3} - p_{\mathrm{c}_x,1} & p_{\mathrm{c}_y,3} - p_{\mathrm{c}_y,1} & p_{\mathrm{c}_z,3} - p_{\mathrm{c}_z,1} \\ \vdots & \vdots & \vdots \\ p_{\mathrm{c}_x,N_\mathrm{c}} - p_{\mathrm{c}_x,1} & p_{\mathrm{c}_y,N_\mathrm{c}} - p_{\mathrm{c}_y,1} & p_{\mathrm{c}_z,N_\mathrm{c}} - p_{\mathrm{c}_z,1} \end{bmatrix} \tag{2}$$

and

$$\begin{aligned} \boldsymbol{u}(k) = &[u_1(k), \ldots, u_{N_\mathrm{c}-1}(k)]^\mathrm{T} \quad \text{with} \quad u_i(k) = r_1^2(k) \\ &- r_{i+1}^2(k) - \left(p_{\mathrm{c}_x,1}^2 - p_{\mathrm{c}_x,i+1}^2\right) - \left(p_{\mathrm{c}_y,1}^2 - p_{\mathrm{c}_y,i+1}^2\right) \\ &- \left(p_{\mathrm{c}_z,1}^2 - p_{\mathrm{c}_z,i+1}^2\right) \quad \forall\, i \in \{1, \ldots, N_\mathrm{c} - 1\}. \end{aligned} \tag{3}$$

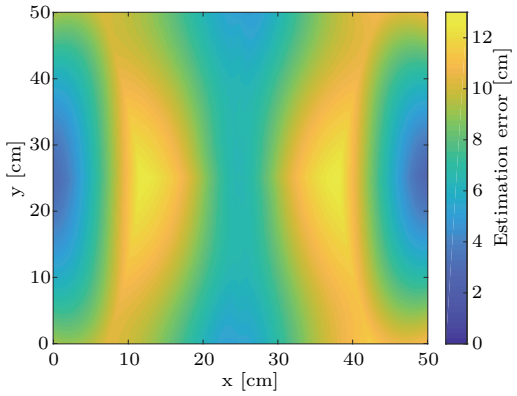

Fig. 2: Maximum simulated error between real and estimated position due to trilateration. The simulated setup is equal to the measurement setup (coil positions and arrangement of the sensor array).

The position of the coil i in x, y, and z position is given by $p_{\mathrm{c}_x,i}$, $p_{\mathrm{c}_y,i}$, and $p_{\mathrm{c}_z,i}$, respectively. The variable $r_i(k)$ describes the radius of the sphere i at the discrete time stamp k. The sphere i describes the shape of the magnetic field of the coil i. The radius is approximated with the matched filter output $\boldsymbol{x}_\mathrm{mf}(k) = [x_{\mathrm{mf},1}(k), \ldots, x_{\mathrm{mf},N_\mathrm{in}}(k)]$ according to

$$r_i(k) = \left(\frac{\tilde{x}_{\mathrm{mf},i}(k)}{\min_i \tilde{x}_{\mathrm{mf},i}(k)} \right)^{-\frac{1}{3}} d_\mathrm{max} \tag{4}$$

with

$$\tilde{x}_{\mathrm{mf},i}(k) = \sqrt{\left(x_{\mathrm{mf},i}(k)\right)^2 + \left(x_{\mathrm{mf},i+N_\mathrm{c}}(k)\right)^2 + \left(x_{\mathrm{mf},i+2N_\mathrm{c}}(k)\right)^2} \tag{5}$$

and the maximum distance d_max between the coils and the points included in the localization area. For applying the trilateration, the shape of the magnetic field is assumed to be spherical. Of course, this is not true and will not lead to the correct position when considering magnetic fields. In Fig. 2 the simulated error between estimated and true position of the sensor array is shown when using the trilateration approach. The positions and orientations of the coils as well as the arrangement of the sensor array are equal to the used measurement setup. The step size of the simulation in each direction (x, y, z) was set to 1 mm and the sensor array was fixed in orientation (0° in roll φ, pitch θ, and yaw ψ). Additionally, the estimated array position was limited to the boundaries of the localization area again. The maximum absolute error for a x-y position pair for all z-positions is shown in the graphic. Localization errors of up to 12.77 cm can occur in this measurement setup with the trilateration approach (considering perfect conditions, e.g. no noise present). But with this initial guess a way smaller localization area can be defined. The estimated position serves as the center of the new localization area and the boundaries are calculated by adding $\pm\Delta d$ to the x, y, and z component of the estimated position. The parameter Δd is set to 13 cm in this

study according to Fig. 2. With the smaller localization area, potential position-orientation-pairs of the sensor array center $\boldsymbol{P}$ can be defined. Based on this, the forward model in form of the leadfield matrix $\boldsymbol{A}$ can be calculated. The leadfield matrix entry of the input variable i and the potential position-orientation-pair j is defined as [6]:

$$a_{ij} = \vec{d}_{\mathrm{p},lj}^{\,\mathrm{T}} \frac{3\,\vec{r}_{\mathrm{p},ij}\,\left(\vec{d}_{\mathrm{c},\lambda}^{\,\mathrm{T}}\,\vec{r}_{\mathrm{p},ij}\right) - \vec{d}_{\mathrm{c},\lambda}\,\left\|\vec{r}_{\mathrm{p},ij}\right\|_2^2}{\left\|\vec{r}_{\mathrm{p},ij}\right\|_2^5}$$
$$\text{with } l = \lceil \frac{i}{N_\mathrm{c}} \rceil \text{ and } \lambda = ((i-1) \mod N_\mathrm{c}) + 1 \quad (6)$$

with the distance $\vec{r}_{\mathrm{p},ij}$ between coil λ and the sensor l that would occur if the sensor array would occupy the potential position and orientation j. The vector $\vec{d}_{\mathrm{p},lj}$ describes the corresponding directivity of the sensor l and $\vec{d}_{\mathrm{c},\lambda}$ the orientation of the coil λ. The estimated position and orientation of the sensor array is calculated by minimizing the cost function [4]:

$$\min_j \sum_{i=1}^{N_\mathrm{in}} \left(\frac{a_{ij}}{\max_i |a_{ij}|} - \frac{x_{\mathrm{mf},i}(k)}{\max_i |x_{\mathrm{mf},i}(k)|} \right)^2 \quad (7)$$

The localization algorithm following the trilateration is iteratively repeated and a Kalman filter is connected consecutively to smooth the results as described in [6].

3 Measurements and Results

For successfully localizing the ultrasound head, the influence of the ultrasound device on the magnetic sensor signals and thus the localization has to be investigated first. In Fig. 3 the power spectral densities (PSDs) of one fluxgate sensor are depicted, once with the ultrasound device switched on and once with the ultrasound device switched off. Additionally, the PSDs are shown once with the coils transmitting orthogonal signals and once without. As can be seen in the graphic, distortions in the lower frequency range occur when turning on the ultrasound device. However, this is not a problem, since the coil signals with frequencies between 610 Hz and 990 Hz are not affected by this as can be seen in Fig. 3b.

Now that an influence from the ultrasound device on the localization has been ruled out, the magnetic 3D sensor (and thus the ultrasound head) will be localized at some fixed position-orientation-pairs as shown in Fig. 4a. The results are shown in Fig. 4b. The localization area is of size 50 cm × 50 cm × 20 cm and the orientation of the sensor can be determined in each angle between $-90°$ and $90°$. The accuracy of the localization is defined as the mean absolute distance between real and estimated sensor position-orientation-pair over time. This leads to a mean accuracy of 2.85 cm and $8.94°$ over all considered measurement positions. This is sufficient for the first simple applications. Measurement position

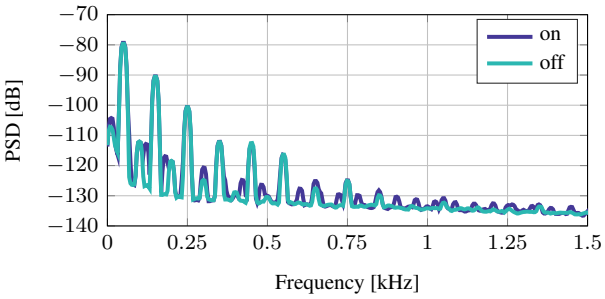

(a) Without coils transmitting signals.

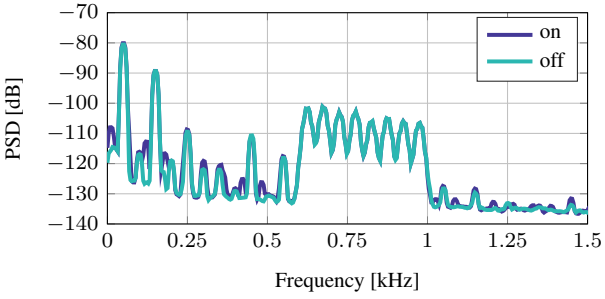

(b) With coils transmitting orthogonal signals in the frequency range between 610 Hz and 990 Hz.

Fig. 3: Power spectral densities of one fluxgate sensor - once with ultrasound device switched on and once off.

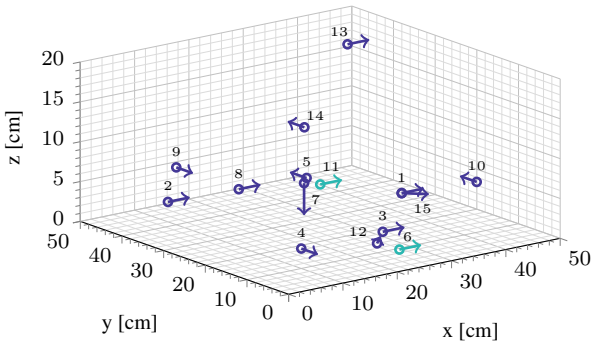

(a) Fixed position-orientation-pairs of the magnetic 3D sensor. The orientation of the sensor array is denoted by the arrow direction. The brighter colouring indicates a rotation by $\varphi = -90°$.

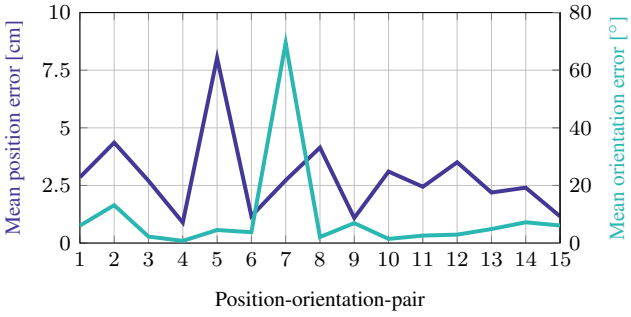

(b) Localization results for the 10 different position-orientation-pairs shown in **(a)**.

Fig. 4: (a) Position-orientation-pairs of the 3D sensor array and **(b)** corresponding localization results for a first proof-of-concept measurement.

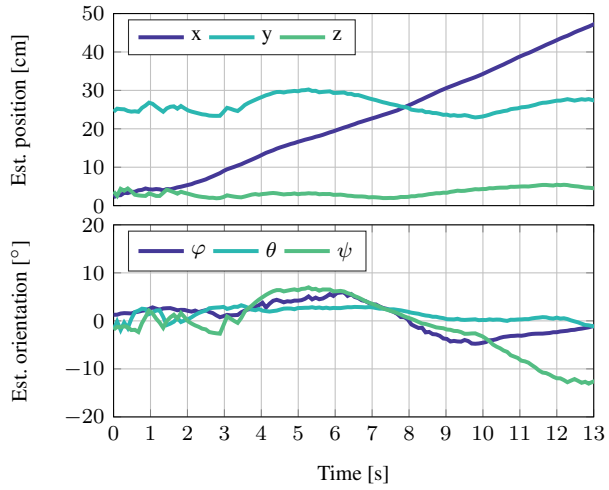

Fig. 5: Localization results of the measurement with the moving sensor.

$k = 7$ was the only measurement with $\theta \neq 0$. When excluding this result, a mean accuracy of $2.86\,\text{cm}$ and $4.62°$ can be achieved.

Due to the real-time capability of the proposed algorithm, the ultrasound probe can of course also be moved during the measurement. The corresponding localization result of a moving measurement is shown in Fig. 5. This result is solely to emphasize the real-time capability of the system. Since no real position was determined during the movement (no continuous speed for manual movements), it can only be stated here that the sensor was moved between $0\,\text{cm}$ and $50\,\text{cm}$ in the x-direction, while it was as far as possible not moved in the y and z position (as well as not rotated). It can be clearly seen, that there are some artifacts/errors occurring during localization. Nevertheless, the movement of the sensor is clearly visible in the localization result.

The complete localization pipeline is run on a PC with an AMD Ryzen 9 3900X processor. The frame size is $16\,\text{ms}$, whereby the localization results (the modules trilateration, iterative localization algorithm and Kalman filter) are only updated every $96\,\text{ms}$ due to the length of the coil signals. The average processing time of the overall localization pipeline is $2.3\,\text{ms}$. The average processing time of the iterative localization algorithm module is the highest with $11.87\,\text{ms}$.

4 Discussion and Future Work

In this contribution a first approach for localizing an ultrasound probe in real time was presented. A sufficient accuracy of about $2.85\,\text{cm}$ and $8.94°$ has been achieved in average in a first proof-of-concept measurement. Additionally, localization results when moving the 3D sensor/ultrasound head were presented, clearly showing the real-time capability of the proposed localization approach. Robustness and accuracy of the algorithm must be further improved in the future. In addition, the influences of a real measurement environment, e.g. a real (metallic) patient bed should be taken into account. In a next step a graphical user interface will be developed, showing the position and orientation of the ultrasound head relative to the patients body. Therefore some guiding points have to be measured/localized in a first step to estimate the body size and thus to correctly place the ultrasonic head on the simulated body (pictograph) of the patient. Additionally, the fluxgate sensors should be replaced by magnetoelectric sensors [4, 6]. The sensors are very small, cost-efficient in production and can be operated in the earth magnetic field [4]. Since the 3D sensor is so far only glued on the ultrasonic head, an integrated sensor in the ultrasonic head would be the long-term-goal.

Acknowledgment: The authors would like to thank Alexander Teplyuk for building the coil amplifier.

Author Statement

Research funding: This work was funded by the German Research Foundation (Deutsche Forschungsgemeinschaft) via the collaborative research center CRC 1261 “Magnetoelectric Sensors: From Composite Materials to Biomagnetic Diagnostics”. Conflict of interest: Authors state no conflict of interest. Informed consent: Informed consent has been obtained from all individuals included in this study. Ethical approval: The conducted research is not related to either human or animal use.

References

[1] Cai Q, Peng C, Prieto J, Rosenbaum AJ, Stinger JSA, Jiang X. A Low-Cost Camera-Based Ultrasound Probe Tracking System: Design and Prototype. 2019 IEEE International Ultrasonics Symposium (IUS), 2019, 997-999

[2] Daoud MI, Alshalalfah A, Awwad F, Al-Najar M. Freehand 3D ultrasound imaging system using electromagnetic tracking. 2015 International Conference on Open Source Software Computing (OSSCOM), 2015, 1-5

[3] Prager RW, Rohling RN, Gee AH, Berman L. Rapid calibration for 3-D freehand ultrasound. Ultrasound Med Biol. 1998 Jul;24(6):855-69.

[4] Spetzler B, Bald C, Durdaut P, Reermann J, Kirchhof C, Teplyuk A, et. al. Exchange biased delta-E effect enables the detection of low frequency pT magnetic fields with simultaneous localization. Scientific Reports. 2021; (2021) 11:5269.

[5] Stefan Mayer Instruments. Magnetic Field Sensor FLC 100. Accessed March 17, 2022. https://www.stefan-mayer.com/images/datasheets/Data-sheet_FLC-100.pdf

[6] Bald C, Schmidt G. Processing Chain for Localization of Magnetoelectric Sensors in Real Time. Sensors. 2021; 21(16):5675.

[7] Shih CY, Marrón PJ. COLA: Complexity-Reduced Trilateration Approach for 3D Localization in Wireless Sensor Networks. 2010 Fourth International Conference on Sensor Technologies and Applications, 2010, 24-32